Revision 1

Occurrence of silica polymorphs nanocrystals in tuffaceous rocks, Province of the Mesa Central, Mexico

LIBERTO DE PABLO,[1,*] MERCEDES DOVAL,[2†] ANGEL LA IGLESIA,[3] JESUS SORIANO,[4] AND LOURDES CHAVEZ[5]

[1]Instituto de Geología, Universidad Nacional Autónoma de México, 04510 México D.F., México

[2†]Departamento de Cristalografía y Mineralogía, Facultad de Ciencias Geológicas, Universidad Complutense de Madrid, 28040 Madrid, Spain

[3]Instituto de Geociencias CSIC-UCM, Facultad de Ciencias Geológicas, Universidad Complutense de Madrid, 28040 Madrid, Spain

[4]Laboratorio Central de Estructuras y Materiales CEDEX, Ministerio de Fomento, Madrid, Spain

[5]Facultad de Química, Universidad Nacional Autónoma de México, 04510 México D.F., México

* Corresponding author.

Instituto de Geología, Universidad Nacional Autónoma de México

Ciudad Universitaria, 04510 México D.F., México

Tel (+52) 5556224284 Fax (+52) 5556224317

E-mail address: liberto@unam.mx

ABSTRACT

Cristobalite-tridymite blade nanocrystals cemented by SiO_2-glass and tridymite nanocrystals fill separately SiO_2-glass spherules released by explosive volcanism, in rhyolitic tuffs from the Province of the Mesa Central, Mexico. This paper presents the mineralogy of silica polymorphs, occurrence and process of formation in the Province of the Mesa Central. The understanding of the origin of these pure SiO_2-polymorphs, their association with high-temperature minerals, fractionation of magmas and role of volatiles contribute to our knowledge on silica minerals, their technological implications and damaging health effects.

Results indicate that a precursor magma, from which kyanite crystallized, partitioned into an immiscible Fe-rich magmatic liquid that crystallized Fe-cordierite, Fe-amphiboles and fayalite and into a siliceous melt that led to low temperature glasses of 78.22-80.01 wt% SiO_2 and Si/Al ratio 4.07-5.65. Presence of amphiboles, sulfur in cristobalite-tridymite crystals and alunite suggest association of volatiles. The crystallization of silica polymorphs is associated with the dissolution of water vapor and volatiles in the precursor magma, establishing a silicate melt–water system of two critical points, one of them at pressure and temperature near the critical point of water and another close to the critical point of SiO_2, and defining a critical curve between them and supercriticality at pressures and temperatures lower than the critical point of SiO_2. Decreasing the ambient conditions from supercritical to subcritical would have allowed the separation of liquid and gases and the crystallization of cristobalite-tridymite and tridymite nanocrystals. Cristobalite single crystals were not form. Transformation to quartz did not occur. Glasses did not crystallize cristobalite or tridymite. Components in excess of the pure phases precipitated as nanoparticles of siliceous glass forming agglomerates, some containing iron hydroxides and alunogen.

Keywords: Silica polymorphs, cristobalite, tridymite

INTRODUCTION

Mineral nanoparticles are released into the atmosphere in aerosols and mineral dusts of variable composition, mineralogy and size distribution by explosive volcanic eruptions (Guo et al. 2004; Reich et al. 2010). They receive attention due to their importance in Earth systems (Hochella 2008; Hochella et al. 2008), as agents of elemental

transport, their technological applications, their unique properties derived from their nano dimensions and their deleterious health effects (Horwell and Baxter 2006). Among the mineral nanoparticles, silica polymorphs are of particular interest because of their limited abundance, technological applications and negative effects on human health. This paper will discuss the mineralogy and formation of nanoparticles of silica polymorphs from the Province of the Mesa Central in Mexico. The significance of nanoparticles stems from the small number of atoms in the particle, a large fraction of which is at or near the surface and significantly modifies the particle's structure, reactivity and properties relative to the bulk material (Banfield and Zhang 2001; Hochella 2008).

Among silica minerals, nanoparticles of β-cristobalite have been recognized in volcanic ash from the Soufrière Hills Volcano in Montserrat, in the British West Indies (Woods 1995; Baxter et al. 1999) and in the respireable fraction of rhyolitic ash from the Chaitén Volcano in the Chilean Patagonia (Reich et al. 2010). They crystallize in the form of fibers from high-temperature reaction in the vapor phase between silica glass and reducing carbon monoxide released during eruption (Mori and Notsu 1997). In an attempt to explain the cristobalite formation mechanism, the syntheses of amorphous silica by laser ablation of mixtures of Si, SiO_2 and Fe, thermal oxidation of Si, oxidation of Si vapors and hydrothermal approaches were considered (Yu et al. 1998; Zhu et al. 1998; Wang et al. 2002; Hu et al. 2003; Palermo and Jones 2004; Zhu et al. 2005). α-Cristobalite was prepared by cooling β-cristobalite synthesized from fumed silica and activated charcoal at 1200 °C to ~240 °C (Hatch and Ghose 1991; Swainson et al. 2003; Deepak et al. 2004). Nanoparticles of tridymite, another silica polymorph, have received less attention than nanoparticles of cristobalite and are not regularly mentioned in the technological and mineralogical literature, which usually refers to tridymite crystals of minute dimensions. Cristobalite and tridymite were first discovered in obsidian glass from Cerro San Cristobal, in Pachuca, Hidalgo, and in the Santin Mine, in Santa Catalina, Guanajuato, in Mexico (Frondel 1962). Since this discovery, many localities worldwide have been added to this list, including some having large crystals (Anthony et al. 2001). The health hazards of silica minerals and volcanic ash have been reviewed (Horwell et al. 2003; Horwell and Baxter 2006).

This paper presents the mineralogy of nanoparticles of silica polymorphs in rhyolitic tuffs from the Province of the Mesa Central, Mexico, discussing the mechanism and process of formation. Additionally, the tuffs experienced a secondary process of zeolitization which will not be discussed in the present paper.

MATERIALS AND METHODS

Materials

The tuffs discussed herein are part of the Tertiary volcanic province that extends over the Province of the Mesa Central, in the states of Zacatecas and Aguascalientes in México. The Mesa Central is bounded to the west by the Province of the Sierra Madre Occidental, a thick sequence of Tertiary volcanoes that extends from the northwest to the southeast with a southern limit of the Province of the Eje Neovolcanico; to the E, the Mesa Central limits with the Province of the Sierra Madre Oriental.

In the Tertiary, a magmatic arc resulting from convergent tectonics in occidental Mexico developed the volcanic package that began forming the Sierra Madre Occidental in the Mid-Eocene with rhyolitic flows and ignimbritic events (McDowell and Keizer 1977; McDowell and Clabaugh 1979; Cameron et al. 1980). The Oligocene – Miocene of the Sierra Madre Occidental was developed through two events, one, at the start of the Oligocene, associated with andesites and basaltic andesites that made the lower andesitic sequence, and one during the Upper Oligocene-Lower Miocene involving an over-800-m thick sequence of rhyolite-ignimbrites and rhyolitic tuffs (McDowell and Keizer 1977; Damon et al. 1981). The Mid Miocene is the source of the andesites associated with the Eje Neovolcanico. The geology of the Province of the Mesa Central has been presented in several maps (Servicio Geológico Mexicano 1998, 2007a, 2007b).

The area of study extends approximately 25000 sq km, between 103°40' – 102°22' W longitude and 22°00' – 21°15' N latitude (Fig. 1). The dominant lithology is the rhyolitic tuff and Oligocene-Miocene rhyolite – ignimbrite, associated with the volcanism of the Sierra Madre Occidental. Exposed in this area are Miocene andesites and basalts, Pliocene calcareous conglomerates and shales and Pliocene conglomerates (Fig. 1). The rhyolitic tuffs were sampled at different locations southeast of Jalpa between Jalpa and Nochixtlan, northeast of Jalpa between Jalpa and Calvillo and east of Calvillo (Fig. 1). The tuff located 20 km northeast of Jalpa between Jalpa and Calvillo, at 102°50' W longitude and 21°12' N latitude, 1350 m elevation, has the highest content of silica polymorphs (Location 3, Fig. 1). Tuffs from other locations correspond predominantly to zeolitized tuffs.

Methods

The mineralogy and petrography of the tuffs were determined by optical microscopy using thin sections and oil-immersion methods. X-ray powder diffraction (XRD) analyses were performed using a Siemens diffractometer with filtered CuKα radiation on powdered bulk material and clay-sized fractions scanned at $1^{o}\,2\theta\ min^{-1}$; clay minerals

were further characterized from oriented mounts analyzed before and after glycolation. Whole-rock major and trace elements analyses were performed by X-ray fluorescence (XRF) on bulk powders fused as glass beads. The total Fe was analyzed by XRF and calculated as FeO; methods to differentiate Fe^{3+} from Fe^{2+} were not considered. The separation of Fe^{2+} and Fe^{3+} in amphiboles was accomplished by calculation. Loss on ignition was determined by wet chemistry.

The morphology, microtexture and composition of minerals and glasses were initially determined by scanning electron microscopy (SEM) at 25 kV operating voltage, coupled with energy dispersive X-ray (EDX) analysis on unpolished fragments that were carbon-coated when analyzed for composition and gold-coated when studied morphologically. More precise studies were performed by high resolution scanning electron microscopy (HRSEM) using a JEOL 2000FX scanning electron microscope operated at an acceleration voltage of 200 kV and equipped with a double inclined sample holder with a resolution of 3.1 Å and an EDX Oxford ISIS spectrometer with a resolution of 136 eV at 5.39 keV. High-resolution transmission electron microscopy (HRTEM) studies were performed using a JEOL 3000FX metallographic microscope operated at an acceleration voltage of 300 kV. The chemical compositions determined by EDX were obtained from selected areas of uniform morphology and mineralogy that were presumably larger than the cross section of the incident electron beam; analyses were calibrated against selected mineral reference materials. Lattice imaging by electron diffraction was useful to recognize structural order in agglomerates of nanoparticles.

RESULTS

The dominant lithology in the area is an assemblage of ignimbrite and rhyolitic tuffs of Oligocene-Miocene age (Fig. 1). Variations in the mineralogy and chemical composition of the tuffs (Tables 1 and 2) allowed the differentiation of the tuffs into four zones: Zone I, northwest of Nochixtlan, elevation 1880-1780 m (Locations 10, 11, Fig. 1), characterized by vitric material, quartz, feldspar, plagioclase, smectite and comparatively higher contents of Si, Al, K and Na and lower contents of Ca, Mg, ignition loss and Ba; Zone II, northwest of Nochixtlan, elevation 1780-1370 m (Locations 12, 13, 14, Fig. 1), characterized by vitric material, heulandite-clinoptilolite, feldspar, plagioclase, smectite and lower contents of Si, Al, K and Na and higher contents of Ca, Mg, ignition loss and Ba; Zone III, northeast of Jalpa, elevation 1370-1334 m (Location 3, Fig. 1), characterized by vitric material,

cristobalite, tridymite, smectite, heulandite-clinoptilolite, plagioclase, feldspar and lower contents of Al, K, Na, Ca, Mg and Ba and higher contents of Si and ignition loss; Zone IV, northeast of Jalpa, elevation lower than 1334 m, characterized by vitric material, heulandite-clinoptilolite, feldspar, plagioclase, alunite and a chemical composition similar to Zone II (Location 2, Fig. 1). The tuff from Zone III shows the most relevant changes and highest abundance of silica polymorphs. It was selected for presentation in further detail.

The rhyolitic tuff cropping at an elevation of 1350 m 20 km northeast of Jalpa (Location 3, Fig. 1) shows by XRD the presence of cristobalite, tridymite, smectite, heulandite-clinoptilolite, plagioclase and feldspar (Fig. 2, Table 1). Its chemical composition, determined by XRF analysis, indicates lower contents of Al, K, Na, Ca, Mg and Ba and higher contents of Si and ignition loss than other tuffs from the area (Fig.1, Table 2).

High-resolution scanning electron microscopy (HRSEM) of the tuff shows silica glass spherules of ~70 μm diameter with a rough botroidal crustal surface covered by small bubbles of SiO_2-glass and immersed in the vitreous matrix (Fig. 3A, composition 3.30.1 in Table 3). Some spherules are replete with cristobalite-tridymite blade nanocrystals ~600-1000 nm wide and ~60-80 nm thick, cemented, non-oriented, and having thin curved irregular edges with an estimated content of 0.02 S^{6+} per $8O^{=}$ (Fig. 3B, composition 3.28.1 in Table 3). These blade crystals are also packed in lepyspheres that fill vesicles (Fig. 3C, 3E, composition 3.31.1 in Table 3), lay on concave etch pits on heulandite-clinoptilolite crystals (Fig. 3D, composition 3.36.1 in Table 3) or are disperse. Other large SiO_2-glass spherules are filled with tabular elongated tridymite nanocrystals ~30 nm thick and ~200-300 nm long, single and in trillings, non-cemented, free of glass and non-oriented (Fig. 3F, composition 3.29.1 in Table 3). Rare tridymite tabular crystals ~5300 nm long, ~600 nm wide and ~130 nm thick are scattered throughout the tuff (Fig. 3G). Blade crystals are intergrowths sharing the (110) face of cristobalite and the (1010) face of pseudo hexagonal tridymite. Cristobalite did not form.

Among the high-temperature minerals, kyanite well-formed crystals fill vesicles in glass (Fig. 3H, compositions 3.13.1 and 3.13.2 in Table 3). Fe-cordierite occurs in vugs but was not observed associated with kyanite (Fig. 3I, compositions 3.12.1 and 3.12.2 in Table 3) and Fe-amphiboles are dispersed (Fig. 3J, compositions 3.6.1, 3.6.2 and 3.6.3 in Table 3). Fayalite is recognized as thin tabular (Fig. 3K, composition 3.1.1 in Table 3) and hexagonal crystallites in Fe-rich glass (Fig. 3L, composition 3.2.1 in Table 3).

Rhyolitic glasses between 78.22-80.01 wt% SiO_2, free of Na_2O and MgO and having Si/Al 4.07-5.65 and R 0.80-0.85 (R=Si/Si+Al) ratios occur as irregular non-vesicular fragments over 30 μm in size (Fig. 3M, composition 3.4.1

in Table 4), slabs ~150 nm thick and 800 nm long (Fig. 3N, compositions 3.9.1 and 3.9.2 in Table 4), and thinner irregular slabs with round edges (Fig. 3N). These thin slabs occasionally occur oriented around orthogonal empty spaces and are crowned by strings of minute glass bubbles (Fig. 3O, compositions 3.14.1 and 3.14.2 in Table 4). Glass spheres of 50-100 nm in diameter are formed (Fig. 3P, composition 3.11.1 in Table 4). A more siliceous glass of 84.67 wt% SiO_2, no Na_2O and MgO, Si/Al 8.68 and R 0.89, fills the voids between crystals (Fig. 3Q, composition 3.37.1 in Table 4).

The authigenic mineralogy of the rhyolitic tuff includes tabular dachiardite crystals in voids and fissures; dachiardite crystals have Si/Al 5.04-5.86, R 0.83-0.85 and are free of FeO (Figs. 3R, 3S, 3T, compositions 3.32.2, 3.34.1 and 3.35.1 in Table 4) (Passaglia and Sheppard 2001).

Nanoparticles of glass of ~6 nm section form ~80 nm aggregates with compositions of 84.91-94.07 wt% SiO_2 and Si/Al 6.88-19.05 and R 0.87-0.95 ratios, which do not diffract electrons (Fig. 4A, compositions 3.39.1 and 3.40.1 in Table 5). There are Fe-rich conglomerates of nanoparticles of this same siliceous glass and possible ferric oxyhydroxide or oxide that do present electron diffraction images (Figs. 4B, 4D, composition 3.41.1 in Table 5) and there are conglomerates of glass nanoparticles and alunogen-alunite of high Al^{3+} content (Fig. 4C, composition 3.42.1 in Table 5). High-resolution transmission electron microscopy (HRTEM) studies revealed the disordered arrangement of Si atoms in glasses of 73.89-96.66 wt% SiO_2 (Figs. 5A, 5B, and 5C). There are faint indications of cubic proto crystals, possibly of cristobalite, in 86.32 wt% SiO_2 glass (Fig. 5A, composition 3.43.1 in Table 5). Silicon atoms appear disordered with occasional presence of elliptical polysomes in 73.89 wt% SiO_2 glass (Fig. 5B, composition 3.44.1 in Table 5) and Si atoms in 96.66 wt% SiO_2 glass attain some degree of long-range order in ~4.7 Å thick parallel layers, which is approximately the thickness of the tridymite tetrahedral ring, corresponding to the (110) or (010) prisms of tridymite (Fig. 5C, composition 3.45.1 in Table 5).

The empirical formulas of the mineral and glasses in the tuff are presented in Table 6. It is noteworthy that glasses present uniform compositions and Si/Al ratios, are free of sodium and were not directly associated to the crystallization of silica polymorphs; one siliceous glass containing 0.977 Si^{4+} (sample 3.45.1), a high temperature calcium glass, did present faint indication of a stacking sequence that suggested tridymite. The compositions of the high-temperature minerals, glasses and authigenic zeolites (Tables 3, 4, 5) are plotted in Fig. 6. The change in composition from glasses to zeolites is smooth and continuous. Glasses are characterized by Si/Al 40.31-4.07 and R 0.97-0.80 ratios, prevalent K and some Ca, and absence of Na and Mg. When Si/Al<5.86 and R<0.85, zeolite was

192 formed. High-temperature kyanite, Fe-cordierite and Fe-amphiboles maintain Si/Al ratios in the range 3.33-0.46.
193 The Fe contents, which are low in kyanite, increases from 0.74 Fe^{2+} atoms per $8O^{=}$ in Fe-cordierite to a maximum of
194 1.27-2.24 Fe^{2+} atoms in Fe-amphibole; fayalite crystals contain 4.09-4.28 Fe^{2+} atoms and together with the Fe-
195 amphibole do not maintain compositional correlation with the other minerals in the tuff. In the glasses, Fe varies
196 from 0.20 to 0 atoms; the larger amounts may correspond to disseminated oxides or hydroxides (Fig. 6).
197
198 **DISCUSSION**
199
200 This study allowed us to determine the occurrence, characterization, chemistry and mineralogy of silica
201 polymorphs in Oligocene-Miocene rhyolitic tuffs in the Province of the Mesa Central, Mexico.
202 The rhyolitic tuff that crops 20 km NE of Jalpa, elevation 1350 m, contains kyanite in vesicles in glass, which
203 depicts crystallization from homogeneous peraluminous magma with content of modifying plus framework former
204 cations less than the Al content. Fe-cordierite, Fe-amphibole and fayalite of progressively increasing Fe content
205 crystallized from a Fe-rich magmatic liquid immiscible with a Si-rich magma that led to siliceous glasses slightly
206 more potassic and calcic and with lower iron content than the precursor magma. These siliceous glasses were
207 characterized by contents of 80.01 – 78.23 wt% SiO_2, Si/Al 4.62 – 4.07 and R 0.82 – 0.80; a higher temperature
208 glass showed 84.67 wt% SiO_2, Si/Al 8.68, R 0.89, free of iron. Previous studies in the FeO-Fe_2O_3-Al_2O_3-SiO_2 and
209 leucite-fayalite-SiO_2 systems (Roedder 1951; Muan 1957; Muan and Osborne 1965) recognized the existence of a
210 high-temperature immiscibility separating Si-rich Fe-poor from Si-poor Fe-rich liquids; later studies have shown a
211 low-temperature immiscibility gap differentiating a fayalite-tridymite-liquid from a tridymite-fayalite-liquid
212 (Thompson et al. 2007).
213 Cristobalite-tridymite blade crystals cemented by SiO_2-glass and containing traces of sulfur fill SiO_2-glass
214 spherules. Tridymite crystals are loosely packed in SiO_2-glass spherules. If crystallization progressed in an
215 anhydrous environment, the eutectic mixture cristobalite-tridymite-SiO_2-liquid would have formed at ~1470 °C and
216 ~0.030 GPa (Tuttle and England 1955) or at ~1470 °C and ~0.8 GPa (Heaney and Banfield 1993; Klein and Hurlbut
217 1993). This temperature of crystallization was susceptible to variation with pressure (Klein and Hurlbut 1993). The
218 displacement of the (100) cristobalite reflection from 4.027Å to 3.97 Å, could imply crystallization at above-

atmospheric pressures (Dera et al. 2011). Tridymite would have crystallized with glass at corresponding lower temperatures.

However, the crystallinity and purity of polymorphs, the SiO_2-glass cementing cristobalite-tridymite crystals and the absence of glass associated to tridymite and of lower temperature phases depict crystallization from highly pure liquid or gaseous phases. The occurrence of Fe-amphiboles, the traces of sulfur in the cristobalite-tridymite intergrowths and the association of alunogen suggest that volatiles, specifically water vapor and sulfur gases, were present. The solubility of H_2O in SiO_2 or in silicate melts increases strongly with pressure and temperature. The cristobalite liquidus is lowered by water vapor at pressures above ~0.030 GPa (Tuttle and England 1955); tridymite in the presence of as little as 2.3 wt% water and pressures of ~0.040 GPa melts to a hydrous liquid, tridymite and SiO_2-glass at 1200 °C and 0.121 GPa (Tuttle and England 1955).

The behavior of a silicate melt in a hydrous environment can be referred to the system SiO_2-H_2O (Kennedy et al. 1962). In the system there are two critical end-points, one, located near the critical point of water at 374 °C and 0.022 GPa, and another located at 1100 °C and 0.97 GPa. The critical line joints both points. Pure SiO_2 has the critical point at 1700 °C and 0.2 GPa (Guissani and Guillot 1996). Below the critical line, the silicate melt containing volatiles –water- coexists with the aqueous fluid containing the mineral -SiO_2; above the critical line immiscibility does not exist and both phases are undistinguishable. The quartz wet solidus curve terminates at 1100 °C and 0.97 GPa by intersection with the critical line; at higher temperatures, intersection will be expected with the critical point of pure silica at 1700 °C (Hack et al. 2007). Water, even in small amounts, causes a rapid decrease in the temperature and pressure of crystallization of SiO_2 when moving from one critical point to the other. Descent in pressure and temperature will ease the transition from supercritical to subcritical conditions, causing crystallization of pure SiO_2. In the subcritical region, descending temperatures and pressures would differentiate water and gas from cristobalite-tridymite and from tridymite crystals. Agglomerates of minuscule glass particles some associated with iron hydroxides and with alunogen are presumed to have precipitated from residual liquids remaining after the crystallization of the SiO_2-polymorphs. The crystallization of pure cristobalite and tridymite from a vapor phase rather than from silicate melts is supported by the HRTEM data, which did not indicate crystallization from glass and only showed in glass of 96.66 wt% SiO_2 faint indications of Si atoms accommodated in parallel stacks that were ~4.7 Å thick, which is approximately the thickness of the tridymite hexagonal rings (Wennemer and Thompson

1984; Wenk and Bulakh 2004). For structural reasons, cristobalite cannot form parallel layers of hexagonal rings (Heaney and Banfield 1993; Wenk and Bulakh 2004).

Quartz did not occur. High-temperature silica phases associated to volcanic eruptions are known for not transforming to low-temperature phases; the transition of tridymite to quartz requires, in addition to cooling, significant structural changes and breakage of bonds (Heaney and Banfield 1993). Single cristobalite crystals were also not formed. The reducing environment favorable to the reduction of amorphous silica by carbon monoxide to cristobalite as per the reactions SiO_2 (amorphous) + CO = SiO + CO_2 and 2SiO + O_2 = 2SiO_2 (cristobalite) assumed for the crystallization of cristobalite fibers in tuffs from the Soufrière Hills Volcano (Woods 1995; Baxter et al. 1999) and from the Chaitén Volcano in Patagonia, Chile (Reich et al. 2010) did not appear to occur in the Province of the Mesa Central.

ACKNOWLEDGEMENTS

This work was supported by Consejo Nacional de Tecnologia, CONACYT, Project D47075F. The principal author is indebted to DGAPA, Universidad Nacional Autonoma de México, for financial support while on a sabbatical leave. The electron microscopy studies were conducted at the Electron Microscopy Laboratory of the Universidad Complutense and the Laboratorio Central de Estructuras y Materiales CEDEX, Madrid. P. Girón assisted with the analytical work.

REFERENCES CITED

Anthony, J.W., Bideaux, R.A., Bladh, K.W. and Nichols, M.C. (2001) Eds., Tridymite, Handbook PDFs, Handbook of Mineralogy, Mineralogical Society of America, Chantilly, VA 20151-1110, USA. http://www.handbookofmineralogy.org/

Banfield, J.F. and Zhang, H. (2001) Nanoparticles in the environment. In J.F. Banfield and A. Navrotsky, Eds., Nanoparticles and the Environment, Reviews in Mineralogy and Geochemistry, v. 44, p. 1-51, Mineralogical Society of America, Washington.

Baxter, P.J., Bonadonna, C., Dupree, R., Hards, V.L., Kohn, S.C., Murphy, M.D., Nichols, A., Nicholson, R.A., Norton, G., Searl, A., Sparks, R.S.J. and Vickers, B.P. (1999) Cristobalite in volcanic ash of the Soufriere Hills volcano, Montserrat, British West Indies. Science, 283, 1142–1145.

Cameron, M., Bagby, W.C. and Cameron, K.L. (1980) Petrogenesis of voluminous Mid-Tertiary ignimbrites of the Sierra Madre Occidental, Chihuahua, México. Contributions to Mineralogy and Petrology, 74, 271-284.

Damon, P.E., Shafigullah, M. and Clark, K.F. (1981) Evolución de magmaticos en Mexico y su relación con la metalogénesis. Universidad Nacional Autónoma de México, Instituto de Geología Revista, 5, 223-238 (in Spanish).

Deepak, F.L., Gautam-Gundiah, M.S., Govindaraj, A. and Rao, C.N.R. (2004) Crystalline silica nanowires. Journal of Materials Research, v. 19, p. 2216–2220.

Dera, P., Lazarz, J.D., Prakapenka, V.B., Barkley, M. and Downs, R.T. (2011) New insights into the high pressure polymorphs of SiO_2 cristobalite. Physical Chemistry of Minerals, 38, 517-529.

Frondel, C. (1962) Silica minerals, Dana's System of Mineralogy, 7th edition, v. III, p. 259-272.

Guissani, Y. and Guillot, B. (1996) A numerical investigation of the liquid-vapor coexistence curve of silica. Journal of Chemistry and Physics, 104, 7633-7644.

Guo, S., Rose, W.I., Bluth, G.J.S. and Watson, I.M. (2004) Particles in the great Pinatubo volcanic cloud of June 1991: The role of ice. Geochemistry, Geophysics, Geosystems, v. 5, Q05003, doi: 1029/2003GC000655.

Hack, A.C., Thompson, A.B. and Aerts, M. (2007) Phase relations involving hydrous silicate melts, aqueous fluids and minerals. In A. Liebscher and C.A. Heinrich, Eds., Reviews in Mineralogy and Geochemistry, v. 65, p. 129-185. Mineralogical Society of America, Chantilly, Virginia.

Hatch, D.M. and Ghose, S. (1991) The α–β phase transition in cristobalite, SiO_2—Symmetry analysis, domain structure, and the dynamic nature of the β-phase. Physics and Chemistry of Minerals, v. 17, p. 554–562.

Heaney, P.J. and Banfield, J.A. (1993) Structure and chemistry of silica, metal oxides and phosphates. In: G.D. Guthrie and B.T. Mossman, Eds., Health effects of mineral dusts, 28, p. 185-233. Reviews in Mineralogy, Mineralogical Society of America, Chantilly, Virginia.

Hochella, M. F. Jr. (2008) Nanogeoscience: From origins to cutting-edge applications. Elements, 4, 373-379.

Hochella, M.F., Lower, S.K., Maurice, P.A., Penn, R.L., Sahai, N., Sparks, D.L. and Twining, B.S. (2008) Nanominerals, mineral nanoparticles and Earth systems. Science, 319, 1631–1635.

Horwell, C.J., Fenoglio, I., Ragnarsdottir, K.V., Sparks, R.S.J. and Fubini, B. (2003) Surface reactivity of volcanic ash from the eruption of Soufrière Hills volcano, Montserrat, West Indies, with implications for health hazards. Environmental Research, 93, 202–215.

Horwell, C.J. and Baxter, P.J. (2006) The respiratory health hazards of volcanic ash: A review for volcanic risk mitigation. Bulletin of Volcanology, 69, 1–24.

Hu, J.Q., Ziang, Y., Meng, X.M., Lee, C.S. and Lee, S.T. (2003) A simple large scale synthesis of very long aligned silica nanowires. Chemical Physics Letters, 367, 339–343.

Kennedy, G.C., Heard, H.C., Wasserburg, G.J. and Newton, R.C. (1962) The upper 3-phase region in the system SiO_2-H_2O. American Journal of Science, 260, 501-521.

Klein, C. and Hurlbut, C.S. (1993) Manual of Mineralogy, 21st ed, 681 p., John Wiley & Sons, Inc., New York.

McDowell, F.W. and Keizer, R.P. (1977) Timing of Mid-Tertiary volcanism in the Sierra Madre Occidental between Durango City and Mazatlan, Mexico. Geological Society of America Bulletin, 88, 1479-1487.

McDowell, F.W. and Clabaugh, S.E. (1979) Ignimbrites of the Sierra Madre Occidental and their relation to the tectonic history of western Mexico. Geological Society of America Special Paper 180, p. 113-124.

Mori, T., and Notsu, K. (1997) Remote CO, CO_2, SO_2, HCl detection and temperature estimation of volcanic gas. Geophysical Research Letters, 24, 2047–2050.

Muan, A. (1957) Phase equilibrium relationships at liquidus temperature in the system FeO-Fe_2O_3-Al_2O_3-SiO_2 system. Journal of the American Ceramic Society, 40, 420-431.

Muan, A. and Osborn, E.F. (1965) Phase equilibrium among oxides in steelmaking, p. 115-116, Addison-Wesley, Massachusetts.

Palermo, V. and Jones, D. (2004) Formation of nanoclusters on silicon from carbon deposition. Applied Surface Science, 226, 191–196.

Passaglia, E. and Sheppard, R.A. (2001) The crystal chemistry of zeolites. In D.L. Bish and D.W. Ming, Eds., Natural Zeolites: Occurrence, Properties, Applications. Reviews in Mineralogy and Geochemistry, v. 45, p. 70-116. Mineralogical Society of America, Chantilly, Virginia.

Reich, M., Zúñiga, A., Amigo, A., Vargas, G., Morata, D., Palacios, C., Parada, M.A. and Garreaud, R.D. (2010) Formation of cristobalite nanofibers during explosive volcanic eruptions. Geology, 37, 435-438.

Roedder, E. (1951) Low-temperature liquid immiscibility in the system K_2O-FeO-Al_2O_3-SiO_2. American Mineralogist, 36, 282-286.

Servicio Geológico Mexicano (1998) Carta Geológica-Minera Aguascalientes F13-9, escala 1:250000, 1 map.

Servicio Geológico Mexicano (2007a) Carta Geológica de Zacatecas, escala 1:250000, 1 map.

Servicio Geológico Mexicano (2007b) Carta Geológica de Aguascalientes, escala 1:250000, 1 map.

Swainson, I.P., Dove, M.T. and Palmer, D.C. (2003) Infrared and Raman spectroscopy studies of the α–β–phase transition in cristobalite. Physics and Chemistry of Minerals, 30, 353–365.

Thompson, A.B., Aerts, M. and Hack, A.C. (2007) Liquid immiscibility in silicate melts and related systems. In: A. Liebscher and C.A. Heinrich, Eds., Natural Zeolites: Occurrences, Properties, Applications, v 65, p. 99-127. Reviews in Mineralogy and Geochemistry, Chantilly, Virginia.

Tuttle, O.F. and England, J.L. (1955) Preliminary report on the system SiO_2-H_2O. Bulletin Geological Society of America, 66, 149-152.

Wang, Y.W., Liang, C.H., Meng, G.W., Peng, X.S. and Zhang, L.D. (2002) Synthesis and photoluminescence properties of amorphous SiO_x nanowires. Journal of Materials Chemistry, 12, 651.

Wenk, H.R. and Bulakh, A. (2004) Minerals, their constitution and origin, Cambridge University Press, 646 p, Cambridge, England.

Wennemer, M. and Thompson, A.B. (1984) Tridymite polymorphs and polytypes. Schweizer Mineralogische und Petrographische Mitteilungen, 64, 335-353.

Woods, A.W. (1995) The dynamics of explosive volcanic eruptions. Reviews of Geophysics, 33, 495–530.

Yu, D.P., Hang, Q.L., Ding, Y., Zhang, H.Z., Bai, Z.G., Wang, J.J., Zou, Y.H., Qian, W., Xiong, G.C. and Feng, S.Q. (1998) Amorphous silica nanowires: Intensive blue light emitters. Applied Physics Letters, 73, 3076–3078.

Zhu, Y.Q., Hsu, W.K., Terrones, M., Grobert, N., Terrones, H., Hare, J.P., Krotoa, H.W. and Walton, D.R.M. (1998) 3D silicon oxide nanostructures: From nanoflowers to radiolarian. Journal of Materials Chemistry, 8, 1859–1864.

Zhu, Y., Yanagisawa, K., Onda, A. and Kajiyoshi, K. (2005) The preparation of nanocrystallized cristobalite under hydrothermal conditions. Journal of Materials Science, 40, 3829–3831.

358 **FIGURE CAPTIONS**

359

360 **FIGURE 1.** Geological map of the area of study limited between 103°40' – 102°22' W longitude and 22°00'-
361 21°15' N latitude, in the Province of the Mesa Central, states of Zacatecas and Aguascalientes, Mexico. Tuffs were
362 sampled in the vicinity of Nochixtlan, Jalpa and Calvillo; sample locations are indicated by numerals. Location 3
363 corresponds to a tuff with the highest content of silica polymorphs, other locations correspond with zeolitized tuffs
364 (base map from Servicio Geologico Mexicano, 1998, 2007a, 2007b).

365 **FIGURE 2.** X-ray patterns of the rhyolitic tuff from Location 3, showing peaks of cristobalite (4.10 Å, 4.05 Å,
366 3.97 Å, 2.46 Å), tridymite (4.10 Å), smectite (14.99 Å, 4.48 Å, 1.50 Å), heulandite-clinoptilolite (9.08 Å, 7.93 Å,
367 3.97 Å, 2.97 Å, 2.79 Å), plagioclase (3.22 Å, 3.77 Å) and K-feldspar (3.34 Å, 3.22 Å, 3.77 Å).

368 **FIGURE 3.** HRSEM images from the rhyolitic tuff: (A) 1 silica glass spherule (composition 3.30.1 in Table 3);
369 (B) 1 cristobalite-tridymite blade crystals in SiO_2-glass spherule (composition 3.28.1 in Table 3); (C) 1 cristobalite-
370 tridymite blade crystals in lepyspheres packed in vesicle (composition 3.31.1 in Table 3); (D) 1 cristobalite-tridymite
371 blade crystals in lepyspheres on heulandite-clinoptilolite (composition 3.36.1 in Table 3); (E) lepyspheres of
372 cristobalite-tridymite blade crystals; (F) 1 tridymite singles and trillings in SiO_2-glass spherule (composition 3.29.1
373 in Table 3); (G) tridymite lamellar crystal; (H) 1, 2 kyanite crystals in vesicle (compositions 3.13.1 and 3.13.2 in
374 Table 3); (I) 1, 2 Fe-cordierite crystals in vesicle (compositions 3.12.1 and 3.12.2 in Table 3); (J) 1, 2, 3 Fe-
375 amphibole (compositions 3.6.1, 3.6.2 and 3.6.3 in Table 3); (K) 1 thin tabular wedge-shape fayalite (composition
376 3.1.1 in Table 3); (L) 1 thin fayalite crystal in glass (composition 3.2.1 in Table 3); (M) 1 siliceous glass
377 (composition 3.4.1 in Table 4); (N) 1, 2 siliceous glass (compositions 3.9.1 and 3.9.2 in Table 4); (O) 1, 2 siliceous
378 glass (compositions 3.14.1 and 3.14.2 in Table 4); (P) 1 glass spheres (composition 3.11.1 in Table 4); (Q) siliceous
379 glass (composition 3.37.1 in Table 4); (R) clinoptilolite and dachiardite (composition 3.32.2 in Table 4); (S)
380 dachiardite (composition 3.34.1 in Table 4); (T) dachiardite (composition 3.35.1 in Table 4).

381 **FIGURE 4.** HRSEM images of: (A) agglomerate of glass nanoparticles <2 nm size (compositions 3.39.1 and
382 3.40.1 in Table 5); (B) conglomerate of nanoparticles of siliceous glass and possible iron oxyhydroxide
383 (composition 3.41.1 in Table 5); (C) conglomerate of nanoparticles of siliceous glass and alunogen-alunite
384 (composition 3.42.1 in Table 5); (D) electron diffraction image of the conglomerate of sample B.

FIGURE 5. HRTEM images of: (A) possible cubic proto-cristobalite in siliceous glass (composition 3.43.1 in Table 5); (B) polysomes in siliceous glass (composition 3.44.1 in Table 5). (C) stacking sequence of atomic layers in siliceous glass, (composition 3.45.1 in Table 5).

FIGURE 6. Variation of the chemical composition of minerals in the tuff. The SiO_2 polymorphs, siliceous glasses, high temperature minerals kyanite and Fe-cordierite and zeolites show compositional continuity whereas Fe-amphiboles and fayalite deviate from the trend, depicting crystallization from a different magma.

Table 1. Mineralogy of the rhyolitic tuffs from the Province of the Mesa Central

	Location						
	11	10	12	13	14	3	2
Elevation (m)	1880	1780	1478	1440	1370	1350	1334
heulandite-clinoptilolite*	-	-	X	X	X	X	X
cristobalite	-	-	-	-	X	X	-
tridymite	-	-	-	-	X	X	-
quartz	X	X	-	-	-	-	-
smectite	X	X	X	X	X	X	X
plagioclase	X	X	X	X	-	-	X
feldspar	X	X	X	X	X	X	X
alunogen-alunite	-	-	-	-	-	X	X
glass	X	X	X	X	X	X	X

*Analyses by XRD.

Table 2. Chemical composition of the rhyolitic tuffs from the Province of the Mesa Central

	Location						
	11	10	12	13	14	3	2
Elevation (m)	1880	1780	1478	1440	1370	1350	1334
SiO_2 *(wt%)	67.27	73.31	69.76	71.13	64.65	71.49	64.30
TiO_2	0.20	0.21	0.30	0.33	0.37	0.33	0.42
Al_2O_3	16.08	11.49	10.55	10.63	12.34	10.80	13.50
Fe_2O_3	2.10	2.34	2.37	2.91	2.98	1.32	3.16
MnO	0.03	0.12	0.03	0.02	0.07	0.01	0.04
MgO	0.60	0.44	1.36	0.79	1.55	0.43	1.80
CaO	0.67	1.45	2.54	2.31	3.00	1.09	2.44
Na_2O	2.78	1.40	0.95	1.22	0.56	0.64	0.90
K_2O	6.98	5.18	2.30	2.56	2.52	1.86	2.57
P_2O_5	0.05	0.07	0.07	0.01	0.13	0.08	0.07
Ign loss	3.11	3.77	9.97	7.94	12.14	12.05	10.99
Rb (ppm)	233	140	137	122	102	40	114
Sr	39	49	505	522	846	314	398
Ba	495	633	785	1605	1283	747	903
Y	58	80	26	21	37	14	28
Zr	212	175	187	171	264	232	223
Nb	10	11	3	4	8	8	6
V	23	119	32	43	32	34	44
Cr	30	18	21	12	12	8	10
Co	7	5	7	6	6	7	8
Ni	6	10	9	7	9	7	9
Cu	5	5	10	15	11	13	14
Zn	74	74	65	103	86	18	78
Th	14	14	7	6	9	10	10
Pb	13	13	7	8	18	15	14

*Analyses by XRF

Table 3. Composition of minerals from the rhyolitic tuff from Location 3, 20 km northeast of Jalpa

	Composition													
	3.30.1	3.28.1	3.31.1	3.36.1	3.29.1	3.13.1	3.13.2	3.12.1	3.12.2	3.6.1	3.6.2	3.6.3	3.1.1	3.2.1
SiO2	100	100	100	94.87	100	30.62	22.04	44.90	45.24	49.53	42.44	41.14	20.78	22.57
Al2O3	0	0	0	3.27	0	56.47	71.81	34.22	23.00	11.51	11.32	10.46	5.74	5.82
K2O	0	0	0	0.52	0	0.78	0.41	1.72	1.20	0.85	1.05	0.60	1.23	1.15
CaO	0	0	0	0.61	0	0.82	0.31	0.69	0.67	0.85	0.65	0.52	0	0
FeO	0	0	0	0	0	11.32	5.44	18.48	29.89	37.27	44.55	47.28	72.26	70.44
Na2O	0	0	0	0	0	0	0	0	0	0	0	0	0	0
MgO	0	0	0	0.71	0	0	0	0	0	0	0	0	0	0
Si4+	4	4	4	4.08	4	1.42	1.00	2.14	2.30	2.61	2.37	2.33	1.47	1.57
Al3+	0	0	0	0.16	0	3.10	3.84	1.93	1.38	0.71	0.74	0.70	0.48	0.48
K+	0	0	0	0.04	0	0.05	0.02	0.10	0.08	0.06	0.07	0.04	0.11	0.10
Ca2+	0	0	0	0.04	0	0.04	0.01	0.04	0.04	0.05	0.04	0.03	0	0
Fe2+	0	0	0	0	0	0.44	0.21	0.74	1.27	1.64	2.08	2.24	4.28	4.09
Na+	0	0	0	0	0	0	0	0	0	0	0	0	0	0
Mg2+	0	0	0	0.04	0	0	0	0	0	0	0	0	0	0
O=	8	8	8	8	8	8	8	8	8	8	8	8	8	8
Si/Al	0	0	0	25.50	0	0.46	0.26	1.11	1.67	3.68	3.20	3.33	3.06	3.27
Si/(Si+Al)	1	1	1	0.96	1	0.31	0.21	0.53	0.63	0.79	0.76	0.77	0.75	0.77
Si/(Al+Fe)	0	0	0	25.50	0	0.40	0.25	0.80	0.87	1.11	0.84	0.79	0.31	0.34
mineral	gl	cr-tr	cr-tr	cr-tr	tr	ky	ky	co	co	am	am	am	fa	fa

gl glass, cr-tr cristobalite-tridymite, tr tridymite, ky kyanite, co Fe-cordierite, am Fe-amphibole, fa fayalite.

Table 4. Composition of minerals from the rhyolitic tuff from Location 3, 20 km northeast of Jalpa

	Composition									
	3.4.1	3.9.1	3.9.2	3.14.1	3.14.2	3.11.1	3.37.1	3.32.2	3.34.1	3.35.1
SiO_2	79.40	79.36	79.60	78.22	80.01	78.84	84.67	80.69	79.29	78.98
Al_2O_3	11.92	12.18	13.66	16.29	14.77	13.80	8.42	11.85	12.94	13.41
K_2O	1.39	3.14	2.03	3.02	3.25	2.45	5.44	1.79	2.24	1.94
CaO	1.73	1.21	1.77	0.98	1.05	1.66	0.54	4.75	4.48	3.70
FeO	5.57	4.10	2.94	1.49	0.92	3.25	0	0	0	0
Na_2O	0	0	0	0	0	0	0	0	0	0.22
MgO	0	0	0	0	0	0	0	0.91	1.04	1.72
Si^{4+}	3.39	3.40	3.37	3.30	3.37	3.35	3.56	3.40	3.35	3.33
Al^{3+}	0.60	0.61	0.68	0.81	0.73	0.69	0.41	0.58	0.64	0.66
K^{+}	0.08	0.17	0.11	0.16	0.17	0.13	0.29	0.09	0.12	0.10
Ca^{2+}	0.08	0.06	0.08	0.04	0.05	0.08	0.02	0.21	0.20	0.17
Fe^{2+}	0.20	0.15	0.10	0.05	0.03	0.12	0	0	0	0
Na^{+}	0	0	0	0	0	0	0	0	0	0.02
Mg^{2+}	0	0	0	0	0	0	0	0.05	0.06	0.11
$O^{=}$	8	8	8	8	8	8	8	8	8	8
Si/Al	5.65	5.57	4.96	4.07	4.62	4.86	8.68	5.86	5.23	5.04
Si/(Si+Al)	0.85	0.85	0.83	0.80	0.82	0.83	0.89	0.85	0.84	0.83
Si/(Al+Fe)	4.24	4.47	4.32	3.84	4.43	4.14	8.68	5.86	5.23	5.04
mineral	gl	gl	gl	gl	gl	gl	gl	da	da	da

gl glass, da dachiardite.

Table 5. Composition of agglomerates and glasses from the rhyolitic tuff from Location 3, 20 km northeast of Jalpa

	Sample						
	3.39.1	3.40.1	3.41.1	3.42.1	3.43.1	3.44.1	3.45.1
SiO_2	84.91	94.07	13.44	5.11	86.32	73.89	96.66
Al_2O_3	10.52	4.10	3.73	57.67	11.57	14.86	3.04
K_2O	1.17	0.57	0.00	12.07	0.20	0	0
CaO	2.31	0.68	0	0	0.76	0.41	0.30
FeO	0	0	82.82	2.05	0.04	0.20	0
MgO	1.09	0.58	0	0	1.22	2.35	0
Na_2O	0	0	0	0	0	0	0
Si^{4+}	3.51	3.81	0.85	0.33	3.60	3.41	3.91
Al^{3+}	0.51	0.2	0.28	4.45	0.38	0.54	0.10
K^{+}	0.06	0.03	0	1.01	0.02	0	0
Ca^{2+}	0.1	0.03	0	0	0.07	0.04	0.03
Fe^{2+}	0	0	3.93	0.1	0	0.01	0
Mg^{2+}	0.07	0.03	0	0	0.15	0.32	0
Na^{+}	0	0	0	0	0	0	0
S^{6+}	0	0	0	2.83	0	0	0
$O^{=}$	8	8	8	8	8	8	8
Si^{4+}/Al^{3+}	6.88	19.05	3.04	0.07	9.50	6.33	40.31
$Si^{4+}/(Si^{4+}+Al^{3+})$	0.87	0.95	0.75	0.07	0.89	0.86	0.97
$Si^{4+}/(Al^{3+}+Fe^{2+})$	6.88	19.05	0.20	0.07	0.89	6.20	39.10
Mineral	gl	gl	fh	al	gl	gl	gl

gl glass, fh iron oxyhydroxide.

Table 6. Empirical formulas of minerals from the rhyolitic tuff from Location 3, 20 km northeast of Jalpa

3.30.1	glass	SiO_2
3.28.1	cristobalite-tridymite	SiO_2
3.31.1	cristobalite-tridymite	SiO_2
3.36.1	cristobalite-tridymite	$(Si_{1.020}Al_{0.040})\ K_{0.010}\ Ca_{0.010}Mg_{0.010}\ O_2$
3.29.1	tridymite	SiO_2
3.13.1	kyanite	$(Si_{0.887}Al_{0.113})\ (Al_{1.824}Fe^{3+}_{0.175})\ (Fe^{2+}_{0.100}K_{0.031}Ca_{0.025})\ O_5$
3.13.2	kyanite	$(Si_{0.625}Al_{0.375})\ (Al_{2.025})\ (Fe^{2+}_{0.131}K_{0.012}Ca_{0.006})\ O_5$
3.12.1	Fe-cordierite	$(Si_{4.815}Al_{0.185})\ (Al_{4.157})\ (Fe_{1.665}Ca_{0.090})\ K_{0.225}\ O_{18}$
3.12.2	Fe-cordierite	$(Si_{5.175})\ (Al_{3.105}Fe^{3+}_{0.895})\ (Fe^{2+}_{1.515}Ca_{0.090})\ K_{0.180}\ O_{18}$
3.6.1	Fe-amphibole	$(Si_{7.830}Al_{0.170})\ (Al_{1.960}Fe^{3+}_{0.060}Fe^{2+}_{2.980})\ (Fe_{1.850}Ca_{0.150})\ K_{0.180}\ O_{22}\ (OH)_2$
3.6.2	Fe-amphibole	$(Si_{7.110}Al_{0.890})\ (Al_{1.330}Fe^{3+}_{1.376}Fe^{2+}_{2.294})\ (Fe_{1.880}Ca_{0.120})\ K_{0.210}\ O_{22}\ (OH)_2$
3.6.3	Fe-amphibole	$(Si_{6.990}Al_{1.010})\ (Al_{1.090}Fe^{3+}_{1.813}Fe^{2+}_{2.087})\ (Fe_{1.910}Ca_{0.090})\ K_{0.120}\ O_{22}\ (OH)_2$
3.1.1	fayalite	$(Si_{0.735}Al_{0.240})\ (Fe^{2+}_{2.140})\ K_{0.055}\ O_4$
3.2.1	fayalite	$(Si_{0.785}Al_{0.240})\ (Fe^{2+}_{2.045})\ K_{0.005}\ O_4$
3.4.1	glass	$(Si_{0.847}Al_{0.150})\ K_{0.020}Ca_{0.020}Fe_{0.050}\ O_2$
3.9.1	glass	$(Si_{0.850}Al_{0.152})\ K_{0.042}Ca_{0.015}Fe_{0.037}\ O_2$
3.9.2	glass	$(Si_{0.842}Al_{0.170})\ K_{0.027}Ca_{0.020}Fe_{0.025}\ O_2$
3.14.1	glass	$(Si_{0.825}Al_{0.202})\ K_{0.040}Ca_{0.010}Fe_{0.012}\ O_2$
3.14.2	glass	$(Si_{0.842}Al_{0.182})\ K_{0.042}Ca_{0.012}Fe_{0.007}\ O_2$
3.11.1	glass	$(Si_{0.837}Al_{0.172})\ K_{0.032}Ca_{0.020}Fe_{0.030}\ O_2$
3.37.1	glass	$(Si_{0.890}Al_{0.102})\ K_{0.072}Ca_{0.005}\ O_2$
3.32.2	dachiardite	$(Si_{40.400}Al_{6.960})\ (Ca_{2.520}K_{1.080}Mg_{0.600})\ O_{96}$
3.34.1	dachiardite	$(Si_{40.200}Al_{7.680})\ (Ca_{2.400}K_{1.440}Mg_{0.720})\ O_{96}$
3.35.1	dachiardite	$(Si_{39.960}Al_{7.920})\ (Ca_{2.040}K_{1.200}Mg_{1.320}Na_{0.240})\ O_{96}$
3.39.1	glass	$(Si_{0.877}Al_{0.127})\ K_{0.015}Ca_{0.025}Mg_{0.017}\ O_2$
3.40.1	glass	$(Si_{0.952}Al_{0.050})\ K_{0.007}Ca_{0.007}Mg_{0.007}\ O_2$
3.43.1	glass	$(Si_{0.900}Al_{0.095})\ K_{0.005}Ca_{0.017}Fe_{0.001}Mg_{0.038}\ O_2$
3.44.1	glass	$(Si_{0.852}Al_{0.134})\ Ca_{0.010}Fe_{0.004}Mg_{0.080}\ O_2$
3.45.1	glass	$(Si_{0.977}Al_{0.023})\ Ca_{0.006}\ O_2$

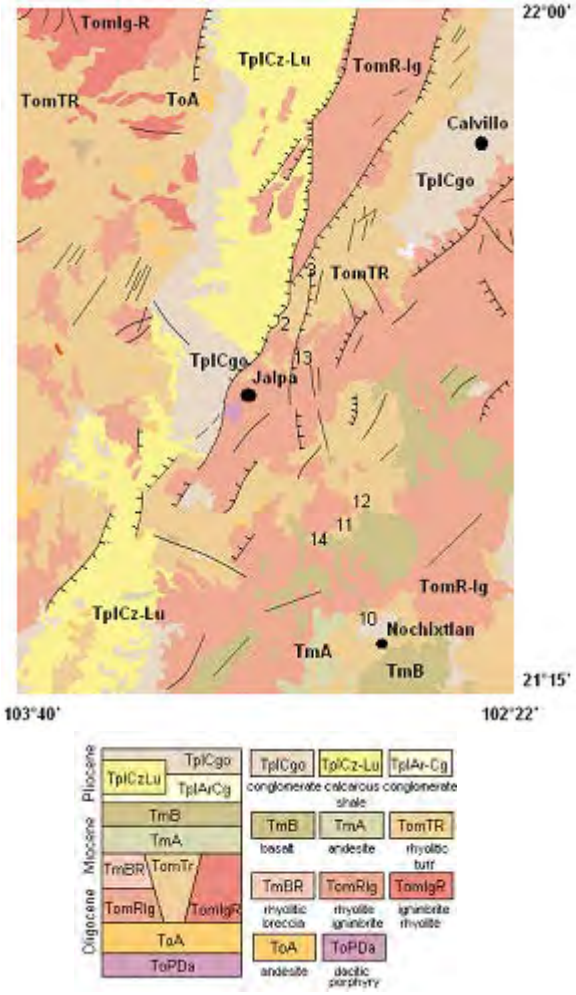

Figure 1

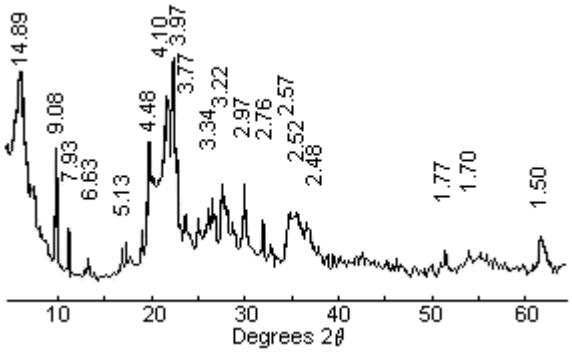

Figure 2

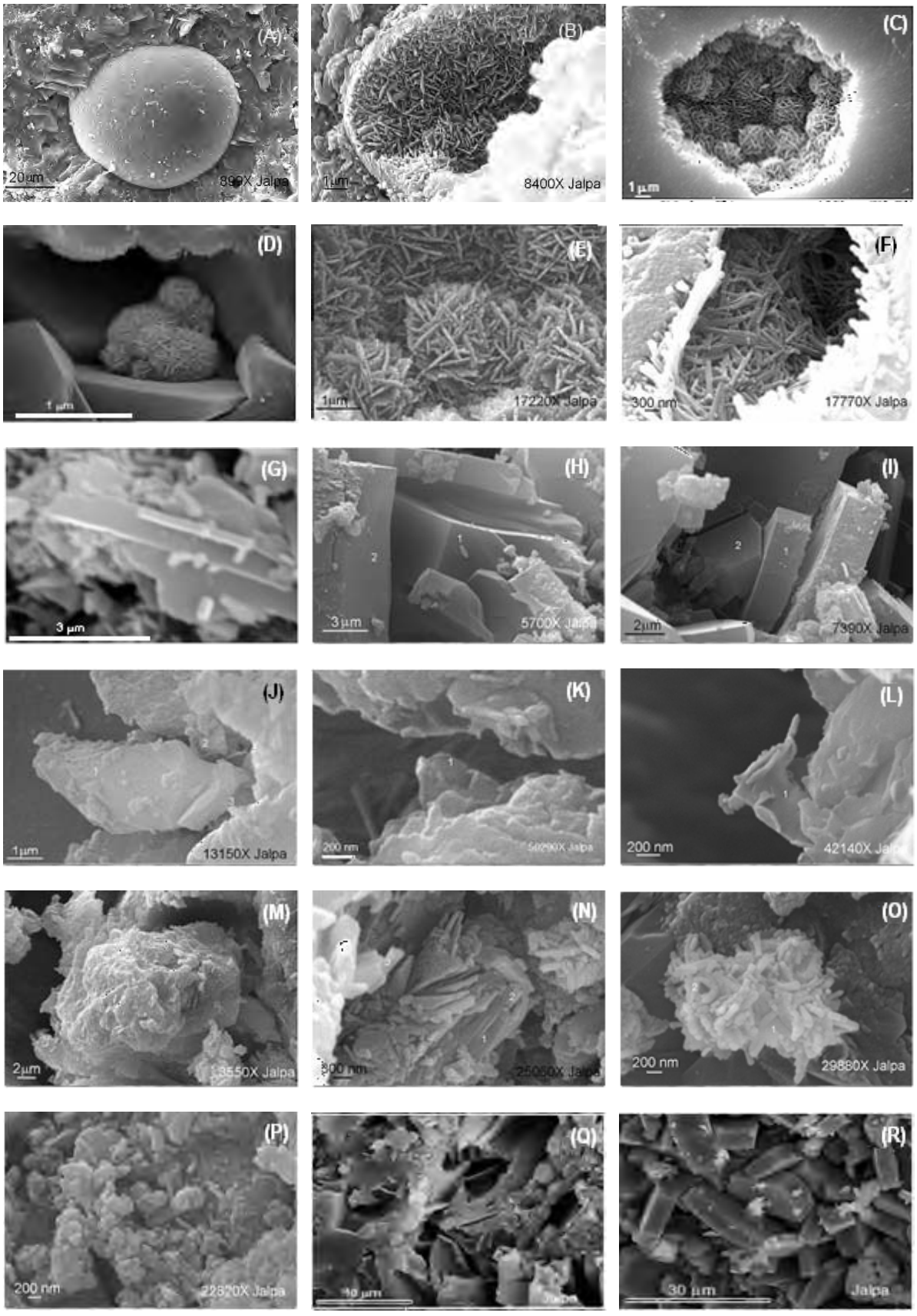

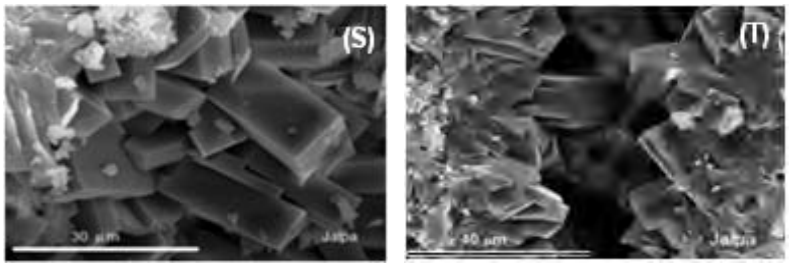

Figure 3

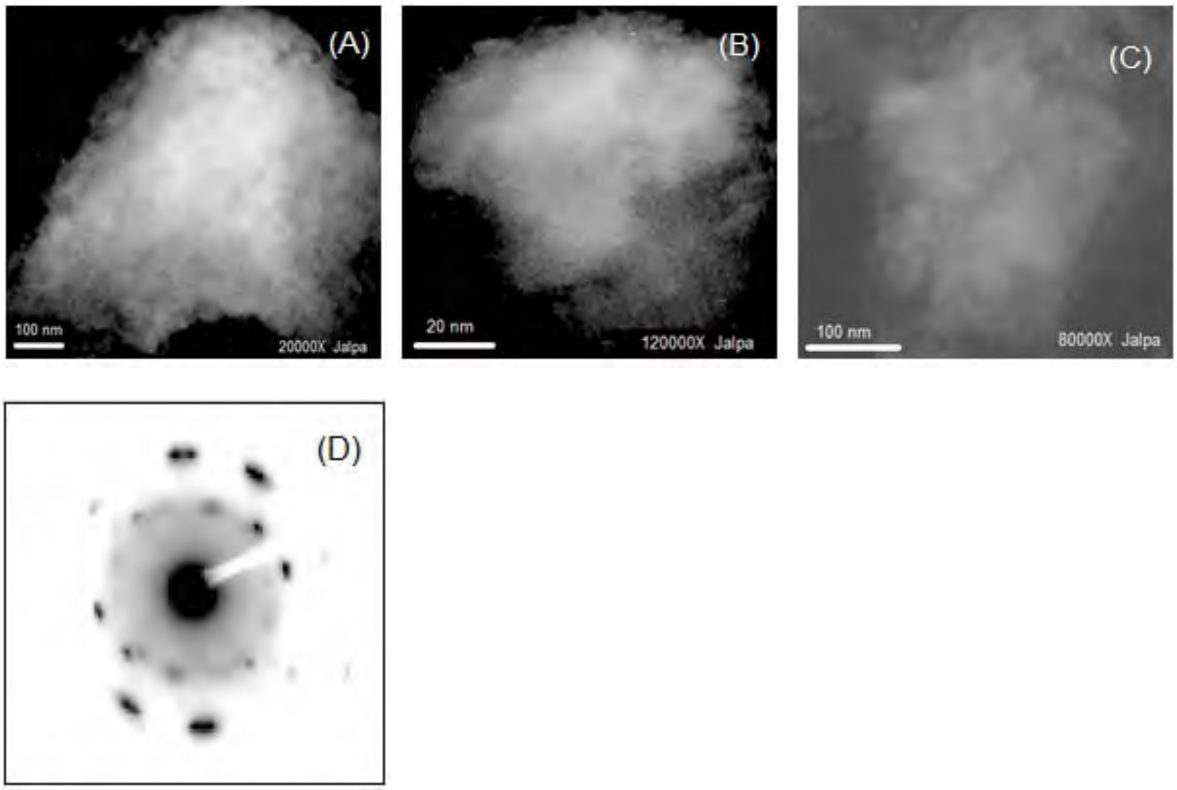

Figure 4

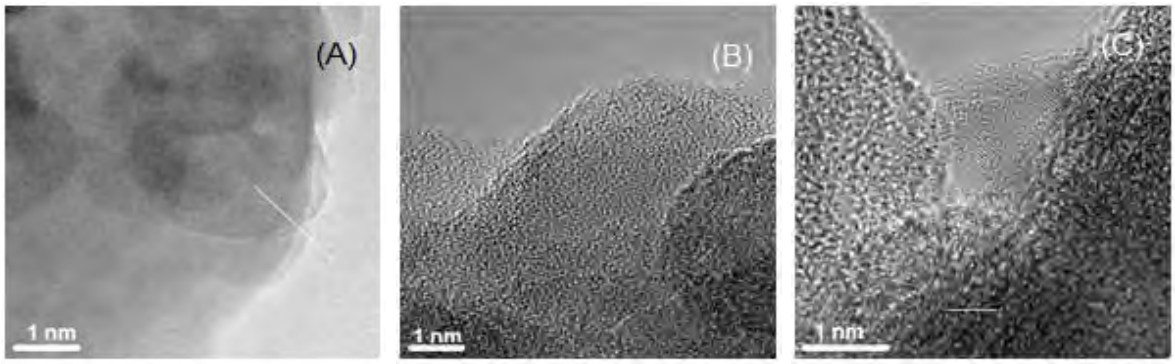

Figure 5

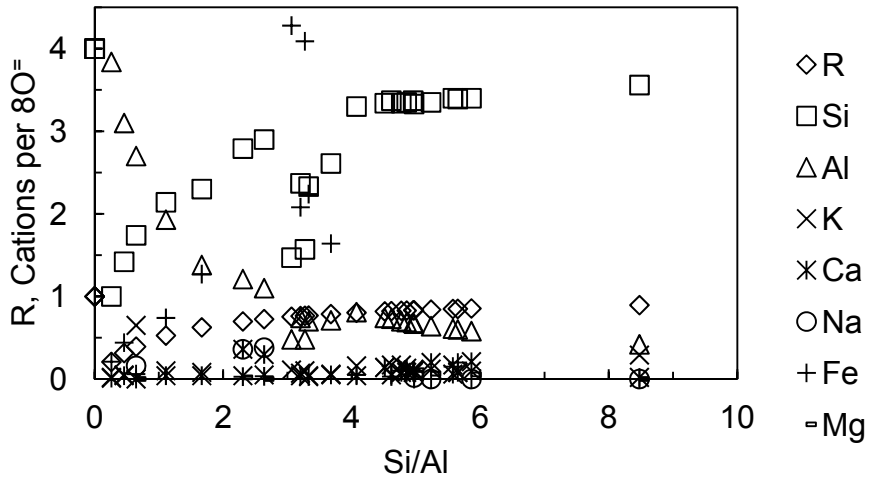

Figure 6